geosciences

MDPI

Article

Assessment of Badlands Erosion Dynamics in the Adriatic Side of Central Italy

Margherita Bufalini [1], Adel Omran [2,3] and Alberto Bosino [4,*]

[1] School of Science and Technology, Geology Division, University of Camerino, Via Gentile III da Varano, 7, 62032 Camerino, Italy; margherita.bufalini@unicam.it
[2] Department of Science and Mathematical Engineering, Faculty of Petroleum and Mining Engineering, Suez University, Suez 43719, Egypt; adelfouad.omran@suezuniv.edu.eg or adel.omran@unipv.it
[3] Department of Earth and Environmental Sciences, University of Pavia, Via A. Ferrata, 1, 27100 Pavia, Italy
[4] Department of Earth and Environmental Sciences, University of Milano-Bicocca, Piazza della Scienza, 1, 20126 Milano, Italy
* Correspondence: alberto.bosino@unimib.it; Tel.: +39-3487942626

Abstract: Badlands are unique soil erosion landforms distributed in numerous geological, geomorphological, and climate contexts in several Mediterranean countries. The aim of this study was to map, classify, and analyze the temporal evolution of the badlands that crop out between the Tesino and Tronto Rivers in the Marche region, Central Apennines (Italy). In this study, 328 badlands landforms were mapped through Google Earth, orthophoto analysis (year 2016), and field surveys. Moreover, badlands were classified from a morphological point of view based on the active processes detected in the field. Additionally, badlands were studied from a lithological point of view, meaning they were strictly related to the soft sedimentary formations of the study area. Subsequently, through the analysis of a 10 × 10 m DEM, the most significant morphometric indices were extrapolated and badlands were classified. Finally, through the orthophotos from 1988, another badlands dataset was created and the area of each landform was compared with respect to the orthophotos from 2016. The multi-temporal air photo analysis, combined with the NDVI results, identified a general reduction trend in badlands areas, with increases in green cover and dense vegetation and changes in badlands morphotypes.

Keywords: badlands (calanchi); inventory map; land use change; vegetation cover; NDVI; Tronto

Citation: Bufalini, M.; Omran, A.; Bosino, A. Assessment of Badlands Erosion Dynamics in the Adriatic Side of Central Italy. *Geosciences* **2022**, *12*, 208. https://doi.org/10.3390/geosciences12050208

Academic Editors: Marten Geertsema and Jesus Martinez-Frias

Received: 1 April 2022
Accepted: 8 May 2022
Published: 13 May 2022

1. Introduction

Soil erosion is one of the most significant land degradation processes worldwide, being able to create spectacular and enduring geomorphological landforms [1,2]. One of the most complex soil erosion landform categories comprises badlands, which are complex sums of splash, rill–interrill, tunneling, gully, and shallow landslides forms and features. 'Calanchi', the Italian term to define badlands, are landforms driven by slope erosion processes, which are deeply and densely crosscut by running water and often developed on unconsolidated or poorly cemented materials [3]. In most cases, they are characterized by steep and unvegetated slopes, high drainage density, and high soil erosion rates. The genesis and evolution of the badlands are complex and still under discussion (e.g., [4]). In Italy, the first studies refer to the work by Azzi [5] and particularly Castiglioni [6,7] who focused on the hilly areas of the Marche and Abruzzo regions (central Italy). In the following years, other authors (e.g., [8–26]) have focused on the study of badlands, and all agree that the main controlling factors on the genesis and evolution of the landforms are the (i) lithology, (ii) climatic factors, (iii) landscape morphology, and (iv) anthropic activity. Badlands landscapes are often associated with arid and semi-arid areas; however, they may also develop in humid areas, such as in central Italy, where high topographic gradients, erodible substrates, and high-intensity storms coexist [27–29]. In addition, in

the literature, wide state-of-the-art studies have been performed on badlands regarding their morphology, triggering factors, geological and structural controls, mineralogical and weathering conditions, and vegetation growth, as well as sediment dynamics modelling and measurements in badland areas in several Mediterranean countries (e.g., [28,30–39]).

The first climatic classification of badlands was performed by Gallart et al. [28], while in the following studies several authors related the precipitation amount and intensity to the vegetation grown, weathering conditions, and erosion processes.

Recently, Nadal-Romero et al. [31] identified the main climate drivers that affect the hydro-geomorphological dynamics in Mediterranean badlands by applying a specific scenario analysis. The abovementioned authors highlight the importance of continuing to monitor the Mediterranean badlands' dynamics in order to understand the future changes.

From here, this study aims to map, classify, and analyze the temporal evolution of the badlands developing between Tesino and Tronto rivers in the Marche region (Central Apennines, Italy) (Figure 1).

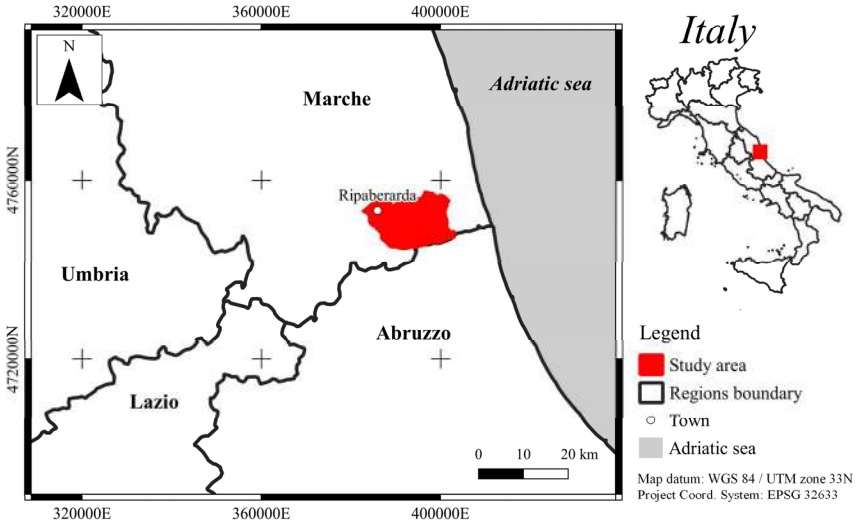

Figure 1. Location of the study area.

The badlands that crop out in the Marche region have undergone significant historical studies [40–50]. These authors assessed the genesis and morphological and morphometrical evolution of these landforms, evaluating the morphodynamical evolution and relation between badlands and the structural setting of the outcropping area. Moreover, they investigated the soil characteristics as well as the chemical and physical properties of the badland lithotypes.

In this work, we want to evaluate the badlands of the Tronto River, and in particular understand variations in the badlands over a period of roughly 31 years through orthophotos and remote sensing techniques. The morphological evolution of the badlands area was studied by several authors in recent years, who highlighted a general shrinking trend of Italian badlands landforms (e.g., [9,43,51–53]), with some cases of areas increasing [54]. Moreover, other studies have confirmed that under certain climate conditions and rainfall amounts, badlands areas will be stabilized [34]. The evolution of the badlands area is related to the land use and land cover changes, amount and intensity of precipitation, weathering conditions, crust protection growth, morphometric characteristics of the basin, and human activity (e.g., [37]). In addition, different phases of badlands evolution may reflect significant environmental changes, such as climate variations and human–environment interactions [10,55]. In times of global change, it is of considerable interest to track environmental changes in different terrains, including badlands, and to properly analyze these processes in order to plan effective strategies for landscape conservation and enhancement [19,52,56–58].

2. Study Area

The study area covers approximately 168 km^2 (of which about 6% is affected by badlands) and is located in the southern Marche region, between the Tesino River to the north and the Tronto River to the south (Figure 1). This area is characterized by a relief that ranges between 17 m a.s.l. near the Tronto river up to 1110 m a.s.l. on the top of Mount Ascensione. Moreover, the area has a humid subtropical climate (Cfa) following the Koppen climate classification [59,60], with an average annual precipitation rate of about 803 mm/year (Center for Ecology and Climatology Experimental Geophysical Observatory http://www.geofisico.it/ (accessed on 19 November 2021) [61]). As specified by Buccolini et al. [43], the study area has been exploited since the 16th century for farming and agricultural purposes, with deforestation and consequent land-use change. Nowadays, the study area is deeply characterized by agricultural fields and vineyards.

The bedrock geology of the area is composed of a Middle Pliocene–Middle Pleistocene succession of different lithotypes in tectonic contact or discordant on the turbidites of the Laga Formation (Messinian) or pelites of the Lower Pliocene [62]. The sedimentary cycle starts with alternating sandstones, calcarenites, and thin, discontinuous conglomeratic levels (Middle Pliocene), intercalated by rare pelitic layers. Throughout the area, powerful pelitic and pelitic–arenaceous units outcrop towards the east, within which sandy–conglomerate clastic levels are present at different stratigraphic heights. The sedimentary cycle ends in correspondence with the coastal area [43]. The bedrock is mostly covered by eluvial–colluvial deposits, mainly of clayey-silt origin, and an extensive presence of alluvial deposits is also visible along the main river valleys.

In the north-western part of the study area, Mount Ascensione stands out as the highest relief of the Periadriatic area of southern Marche (1110 m a.s.l.) and represents the area where the Upper Pliocene [63,64] bedrock is at the highest altitude in Europe.

The bedrock consists of a conglomeratic body, in which at least five sedimentation events can be recognized, alternated with pelites of the Plio–Pleistocene sedimentary cycle, which are transgressive on the underlying Messinian turbidites of the Laga Formation [65].

The lithostratigraphic succession of each level consists of the superimposition, in sequence, of conglomeratic lithofacies and arenaceous and arenaceous–pelitic levels.

Rare dip–slip faults (roughly NW–SE and WSW–ENE-oriented), with weak vertical displacement and similarly oriented joint systems, dislocate the monoclinal structure of the area [66,67].

The morphological setting of the area is driven by the tectonic activity, which is influenced the relief formation and its evolution (e.g., [43]). Moreover, as already observed by numerous authors (e.g., [40,49,65]), microclimatic, lithostratigraphic–structural, and geomorphological factors play a fundamental role in the genesis and development of the badlands morphologies (Figures 2a,b and 3a–c). Several forms of erosion present in the study area can be related to the presence of soft sedimentary bedrock. In particular, badlands represent the dominant landforms that crop out along the monoclinals and cataclinals of the second order of the Tronto River. Moreover, from field observations, a relation between the structural setting of the area and the landform morphology clearly appears. The badlands are developed both on tectonic and erosion triangular facets [68], and often represent the mutual interactions between tectonic activity and erosion processes (Figure 3c,d).

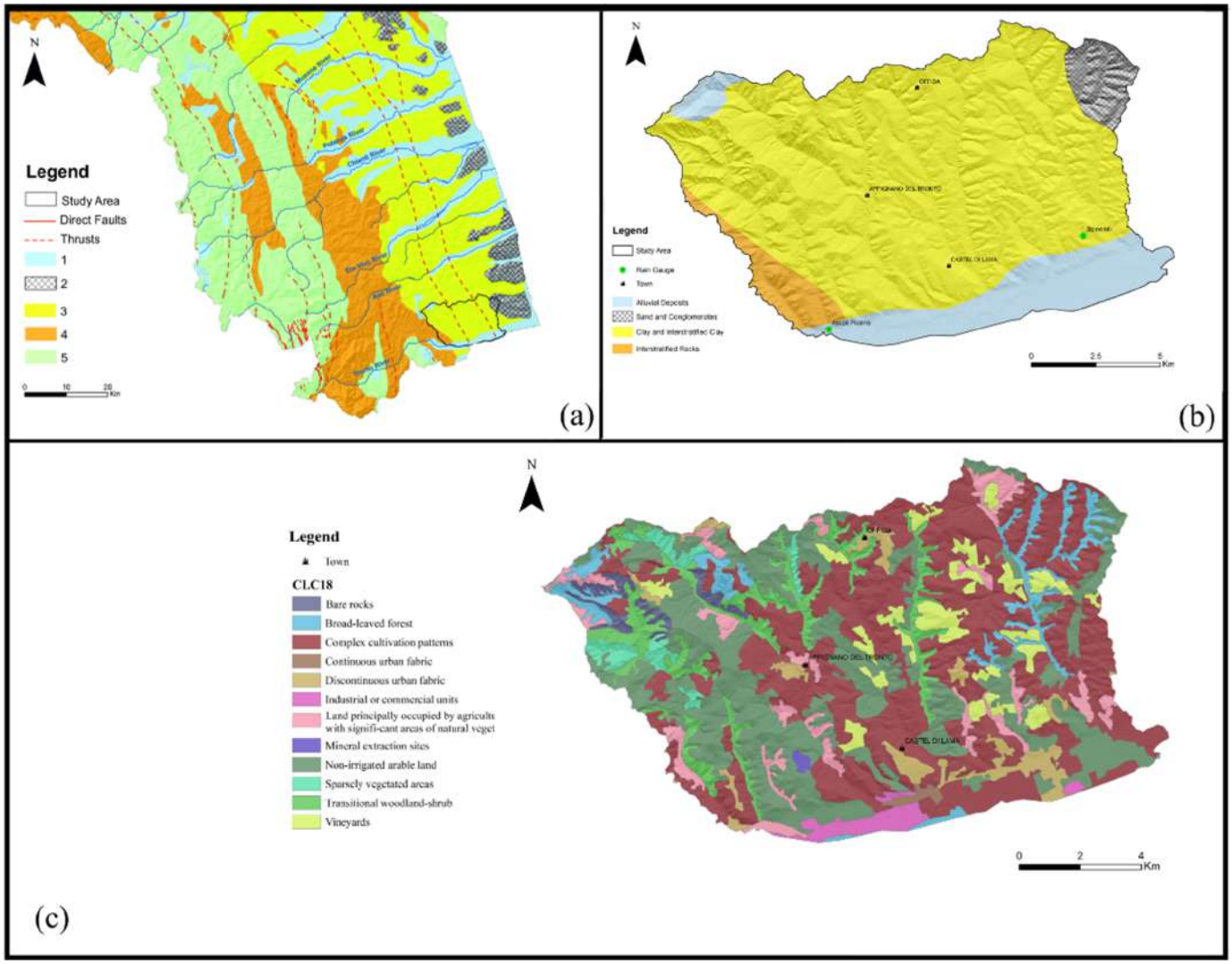

Figure 2. (**a**) Schematic geological map of the southern part of Marche region (Pierantoni et al., 2013 [69]): 1—main continental deposits (Pliocene–Pleistocene–Holocene); 2—sands and conglomerates (Pliocene–Pleistocene); 3—clays and sands (Pliocene–Pleistocene); 4—arenaceous–marly clayey turbidites (late Miocene); 5—limestone, marly limestone, and marls (early Jurassic–Oligocene). (**b**) Geologic map of the study area. (**c**) CORINE Land Cover map.

The badlands of the study area were investigated in the last years because they are an important hotspot for local geological tourism [48]. The badlands of the Tronto Basin show the morphological features of "badlands type A" (Figure 3a) and "badlands type B" (Figure 3b), as described by Moretti and Rodolfi [50] and subsequently by Bosino et al. [9]. The badlands type A have very thin ("knife-edge") ridges separating valleys with a strongly incised "V" shape and arranged in a herringbone pattern (see also Buccolini et al. [43]), as well as a dense drainage pattern. Conversely, badlands type B present wider valleys with softer morphologies, sparse vegetation cover, and the presence of mass movements on which the erosional processes rapidly decrease. As specified by Moretti and Rodolfi [50], other intermediate landforms can occur. Indeed, in the study area, type A badlands are occasionally associated with mud flow processes that smooth the interfluves. In addition, most of the badlands that can be observed in the area are characterized by a sandstone cap, which acts as an erosive base level arresting the erosive processes (Figure 3e). In general, the erosive processes in the area are still active, as demonstrated by several rill–interrill and active gully systems. Finally, in the western part of the study area, several badlands surfaces and isolated badlands can be mapped.

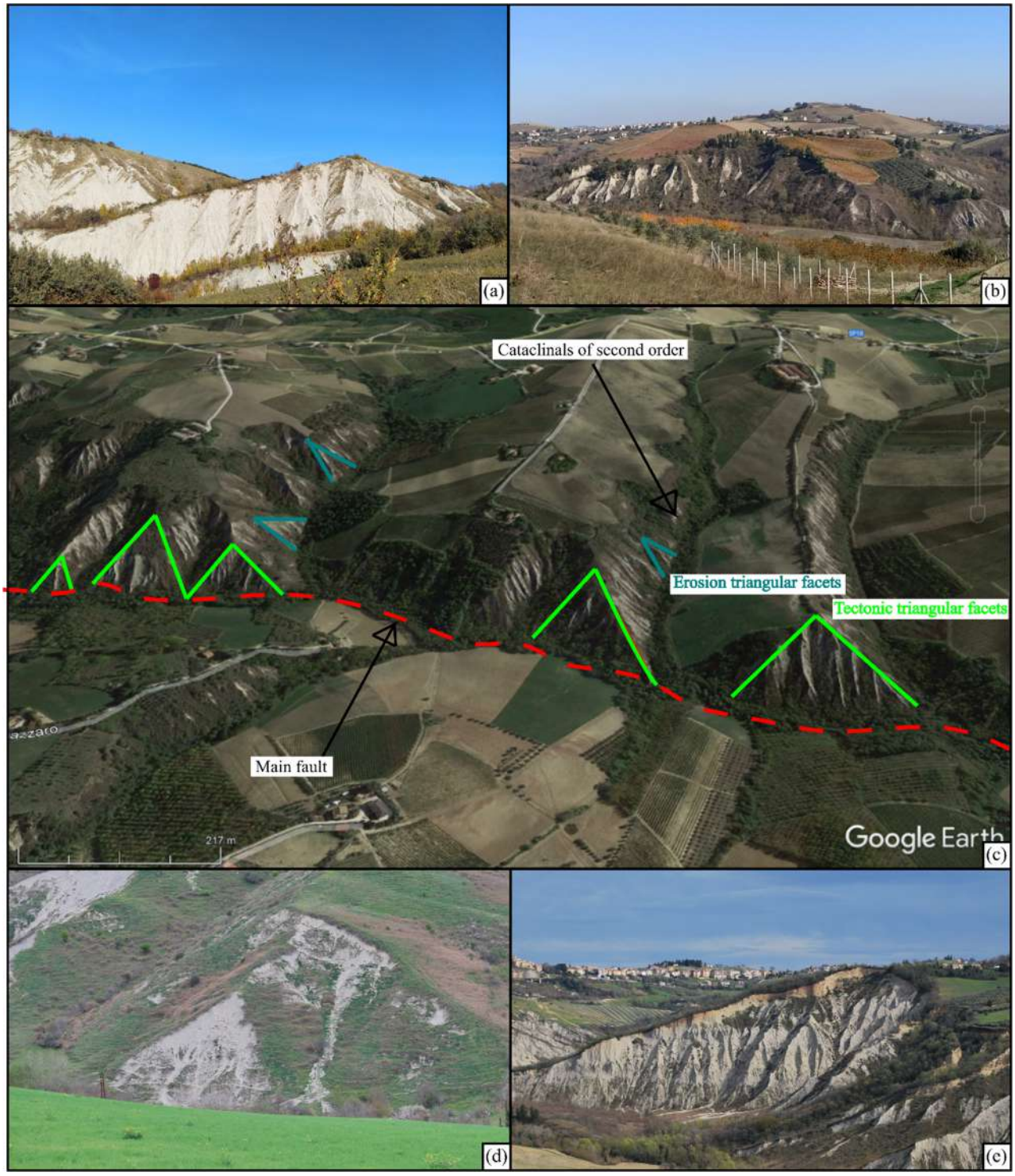

Figure 3. (**a**) Type A badlands, (**b**) type B badlands, and (**c**) facets related to the tectonics on which badlands processes are active and erosional stages. (**d**) Erosive triangular facets shaped by runoff processes and mud flows. (**e**) Sandstone cap layer protecting the badlands.

3. Methods

For the classification of the badlands, the approach used in this study is shown in the flow chart (Figure 4).

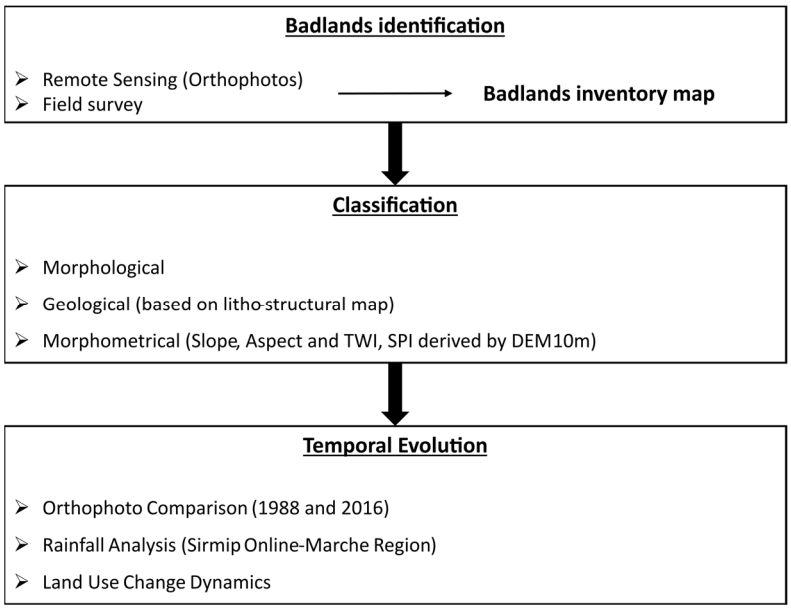

Figure 4. Flow chart illustrating the badlands assessment approach (modified from [9]).

3.1. Badlands Identification

Badlands areas were mapped starting from the orthophotos (year 1988) available from the Marche Region website (https://www.regione.marche.it/Regione-Utile/Paesaggio-Territorio-Urbanistica-Genio-Civile/Cartografia-e-informazioni-territoriali/WMS#Servizi-WMS) (accessed on 19 November 2021) and the orthophotos (year 2016, resolution 20 cm) courtesy of the "Consorzio di Bonifica delle Marche". The badlands areas were initially mapped excluding the vegetation in the surrounding areas and subsequently stored in Shape format using QGIS 3.18.0-Zurich software (https://qgis.org/en/site/) (accessed on 19 November 2021). For each landform, a unique Id, type of badlands, and total area covered by the landforms were associated.

3.2. Badlands Classification

The morphological classification of badlands was carried out following the classification developed by Moretti and Rodolfi [50], who divided the landforms into type A and type B. In addition, in order to find a correlation between the morphology and lithology, the mapped badlands were classified from a lithological point of view using a litho-structural map at 1:10,000 [69].

Subsequently, the most import morphometric indices linked to badlands erosion (e.g., [8,70]), such as the slope, aspect, Topographic Wetness Index, and Stream Power Index [71] values, were derived from a digital elevation model (DEM) with a 10 × 10 m cell, which was freely downloaded from the INGV website (http://tinitaly.pi.ingv.it/) (accessed on 19 November 2021).

Through the SAGA GIS [72], the DEM was initially hydrologically corrected to eliminate sinks through the use of the algorithm proposed by Wang and Liu [73]. Subsequently, the morphometric indices were derived. The single index values were categorized in order to better represent the single variable. The slope values, representing the gradient of the side, were divided into 6 classes (between 0° and 90°); the aspect values, representing the exposition of the slope, were divided into 8 classes (between 0° and 360°); the Topographic Wetness Index (TWI) values, representing the topography control on hydrological processes and the runoff generation potential, were divided into 8 classes; and finally the Stream Power Index (SPI) values, which describes the potential run-off erosion at a given point of the topographic surface [71], were divided into 13 classes.

3.3. Temporal Evolution

To assess the temporal evolution of the landforms, we compared the badlands area of the year 1988 (summer—August) with the 2016 data (summer—June) (Figure 5a,b). Subsequently, a geomorphological survey through field observations was carried out to investigate the causes of badlands area changes, followed by a detailed analysis of precipitation and land use trends. The badlands area variation was evaluated by observing the precipitation trend in the area. In fact, the mean annual precipitation data for two rainfall stations located in Spinetoli and Ascoli Piceno were considered (Figure 2b). The rainfall dataset of the two selected periods (1988 and 2016) was achieved from the Marche Region website (https://www.regione.marche.it/Regione-Utile/Protezione-Civile/Console-Servizi-Protezione-Civile/SIRMIP-online) (accessed on 19 November 2021). Finally, the rainfall percentile analysis was conducted in order to show the influence of the rainfall intensity to evaluate extreme precipitation events [74–78].

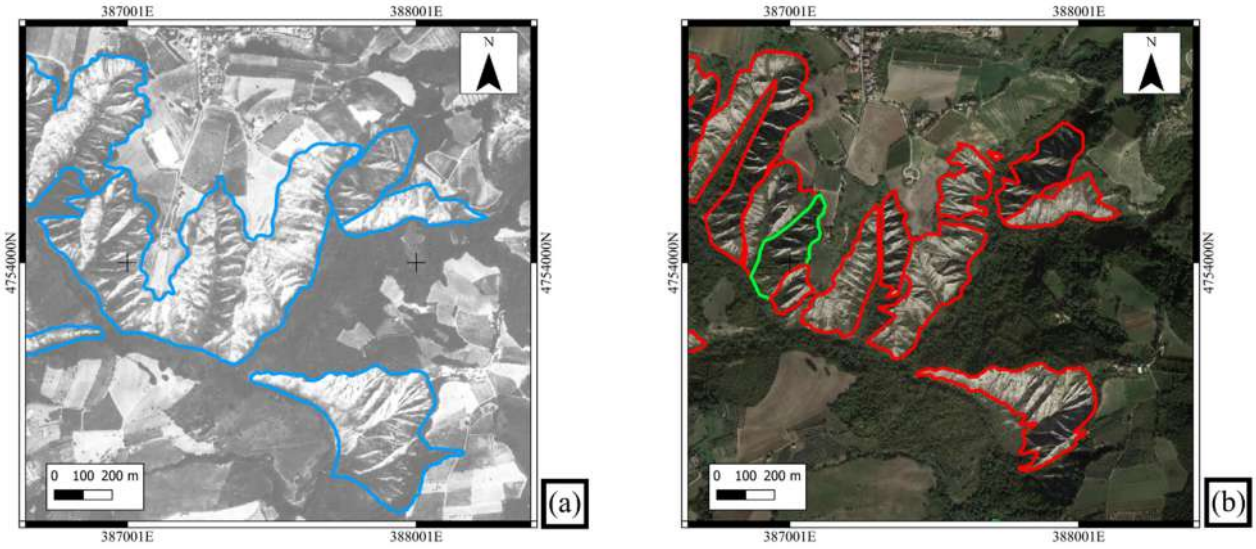

Figure 5. Details of badlands areas in 1988 (**a**) and 2016, red lined badlands Type A, green line, badlands Type B (**b**).

The relationship between changes in vegetation cover and badlands erosion rates has been assessed by numerous authors [9,28,79,80]. In this work, the multitemporal evaluation of vegetation change was assessed through the "CORINE Land Cover" dataset, downloadable from the Copernicus website (https://land.copernicus.eu/pan-european/corine-land-cover, (accessed on 19 November 2021) geometric accuracy, satellite data: CLC1990 $\leq$ 50 m; CLC 2018 $\leq$ 10 m (Sentinel-2)) for the years 1990 and 2018.

Furthermore, through satellite images, we extrapolated the vegetation index, i.e., NDVI (Normalized Difference Vegetation Index), which provides information on the effects of green cover on soil erosion and consequently on the evolution of badlands. In our study, different medium-resolution multi-spectral images recorded during the years 1988 and 2016 were compared to assess spatiotemporal variations. For the derivation of the NDVI, we used the red and near-infrared spectral bands, from the longest available multi-sensor time series. The image selection was based on the following criteria: (i) synchronicity; (ii) lowest cloud cover as catalogued by USGS (2019); (iii) a visual inspection of the images.

Two series of images were recorded from different earth observation satellite platforms over 31 years. The acquisitions were from the Landsat L-5 Thematic Mapper © August 1988 (LANDSAT/LT05/C01/T1_SR/LT05_190030_19880816) and Landsat8 of August 2016 (LANDSAT/LC8_L1T/LC81900302016242LGN00), respectively, at 30 m resolution. All acquired images were pre-georeferenced to UTM zone 33 with datum WGS 84 and orthorectified using a digital elevation model. The images and NDVI data were processed in this study using Google Earth Engine (GEE). GEE is a cloud-based geospatial processing

platform that provides online access to its archived datasets. In this study, the JavaScript application programming interface (API) was used for calling, pre-processing, mosaicking, and processing. The images were then corrected and filtered to obtain cloud-free products.

The NDVI data computed from the near-infrared and red calibrated images of each year provided a representation of the green vegetation cover distribution. We used the following bands for the NDVI calculation provided by the different platforms: (a) band 3 (red) and band 4 (near-infrared) from the Landsat 5 images; (b) band 4 (red) and band 5 (near-infrared) from the Landsat 8. The NDVI values were classified into three equal intervals, then used to compare the images and evaluate the evolution of the vegetation in the study area.

4. Results and Discussion

The main objective of the study was to provide an inventory of the badland's landforms present in the area investigated together with an in-depth analysis of their geological, geomorphological, and temporal characteristics.

Initially, 328 badlands were mapped from the 2016 orthophotos (Figure 6). The badlands covered an area measuring 7.04 km^2. Subsequently, a second badlands inventory was formed starting from the orthophotos from 1988, observing an eroded area measuring 10.34 km^2. From the badlands area comparison, it is possible to observe a decrease of approximately 31.7% in roughly 31 years.

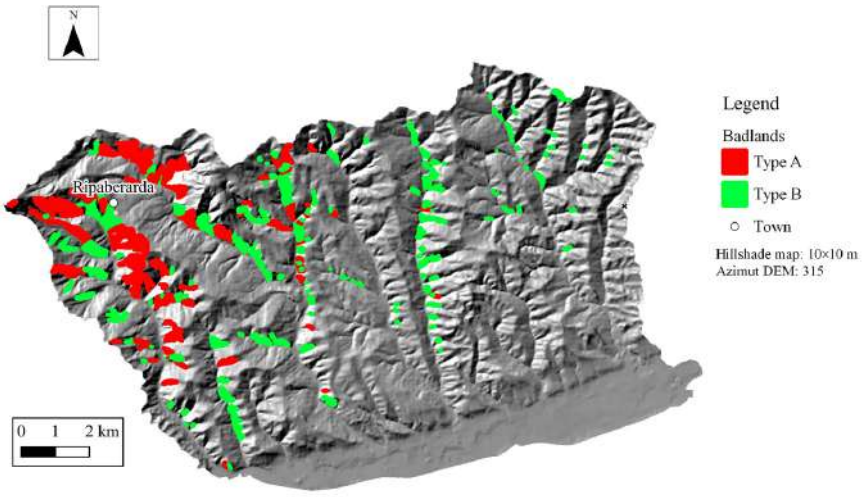

Figure 6. Inventory map of badlands cropping out between the Tesino and Tronto River Basins.

As previously mentioned, the badlands were classified into types A and B based on their morphological characteristics. Relative to the year 2016, type A badlands represent 57% of the area and cover 4.07 km^2, while 43% of the area is represented by type B badlands, covering 3 km^2. In addition, from the comparison of the two orthophoto datasets for the years 1988 and 2016 (Figure 5), one can clearly detect a general reduction in type A badlands and an increase in type B badlands. As defined by several authors, i.e., Ciccacci et al. [10], type B badlands represent the natural evolution of type A badlands due to landform smoothing and vegetation growth. In addition, the number of badlands areas increased after 31 years from 284 to 328 due to revegetation, which divided the single landforms (Figure 5). At the same time, a reduction in the eroded area was observed from 10.34 to 7.04 km^2 (Figure 7b,d).

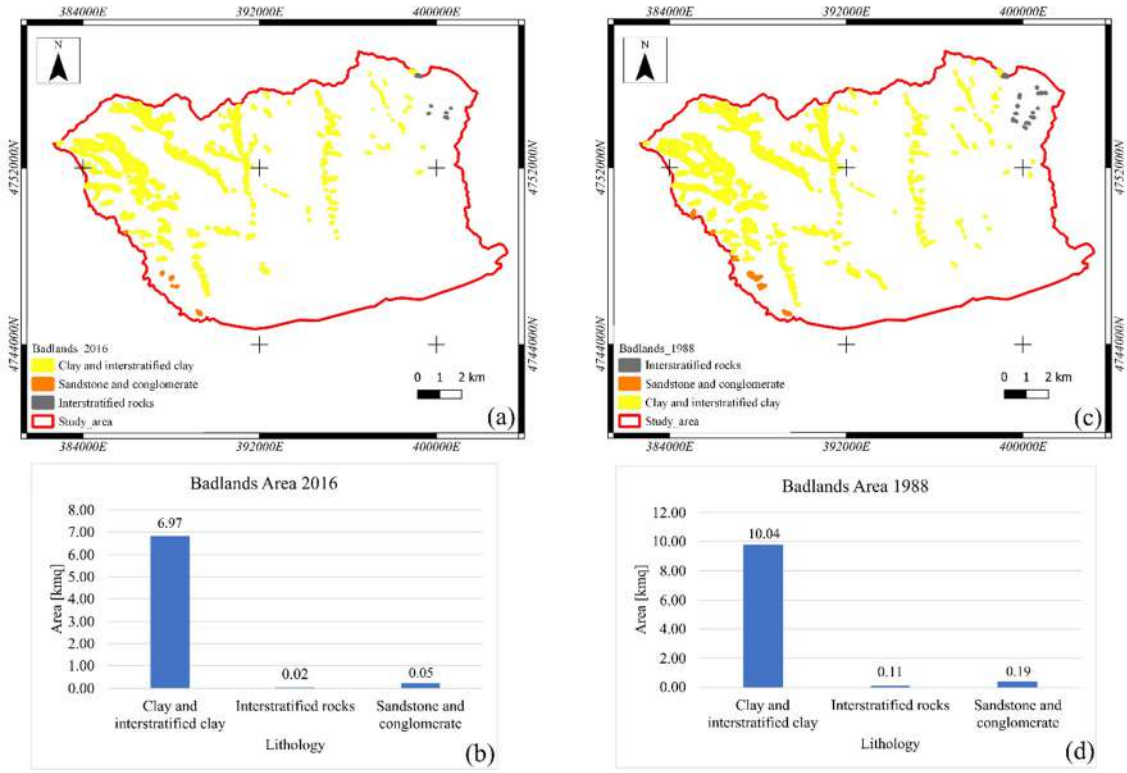

Figure 7. Badlands inventory in 2016 (**a**), lithology distribution in 2016 (**b**), badlands inventory in 1988 (**c**), and lithology distribution in 1988 (**d**).

In addition, observing the lithological distribution of the badlands, it was possible to observe a high concentration of landforms in fine Pliocene clay, marls, and limestone lithotypes. Grain size analyses were conducted on soil samples from some badlands, showing a silty clay loam texture (USDA classification). However, more detailed studies on physical and chemical properties of these soils need to be conducted in order to be statistically significant and to discriminate between type A badlands with and without mud flow processes.

The formation of the badlands and their subsequent development is related to the presence of different geological characteristics, such as well-cemented sandstones alternating with finer and weaker marls and clays. In addition, mass movements, triggered by intense rainfall, induce the formation of erosive processes such as rills and gullies and the subsequent development of badland morphologies.

Moreover, comparing how the lithology has influenced the badlands evolution, it is evident from Figure 7a–d that the coarse lithotypes, i.e., sandstone, bring about a general reduction in the badlands over the 31 years. On the contrary, clay and interstratified clays representing the Pleistocene Fm. bring about an increase in badlands area. This can be explained by the higher permeability of coarse bedrock lithotypes, which facilitate the vegetation growth. Concerning the morphometric analysis, as specified in the previous chapters, four morphometric indices (slope, aspect, TWI, and SPI) were derived from the DEM. The results show that the badlands are mainly south-west facing (180°–225°), have slope angles ranging between 20° and 30° (about 85%), TWI values ranging from 6 to 10 (Figure 8a–c), and variable SPI values (Figure 8d) due to the fact that this parameter measure the erosive power of the streamflow based on the assumption that the discharge is proportional to the specific catchment area [70], while in the study area several badlands cropped out in the facets guided by the structural setting. The obtained results are in good agreement with those observed in the Oltrepo Pavese (Northern Italy) area in [19], in a pilot area in the Modena Province in [12], and partially in [56].

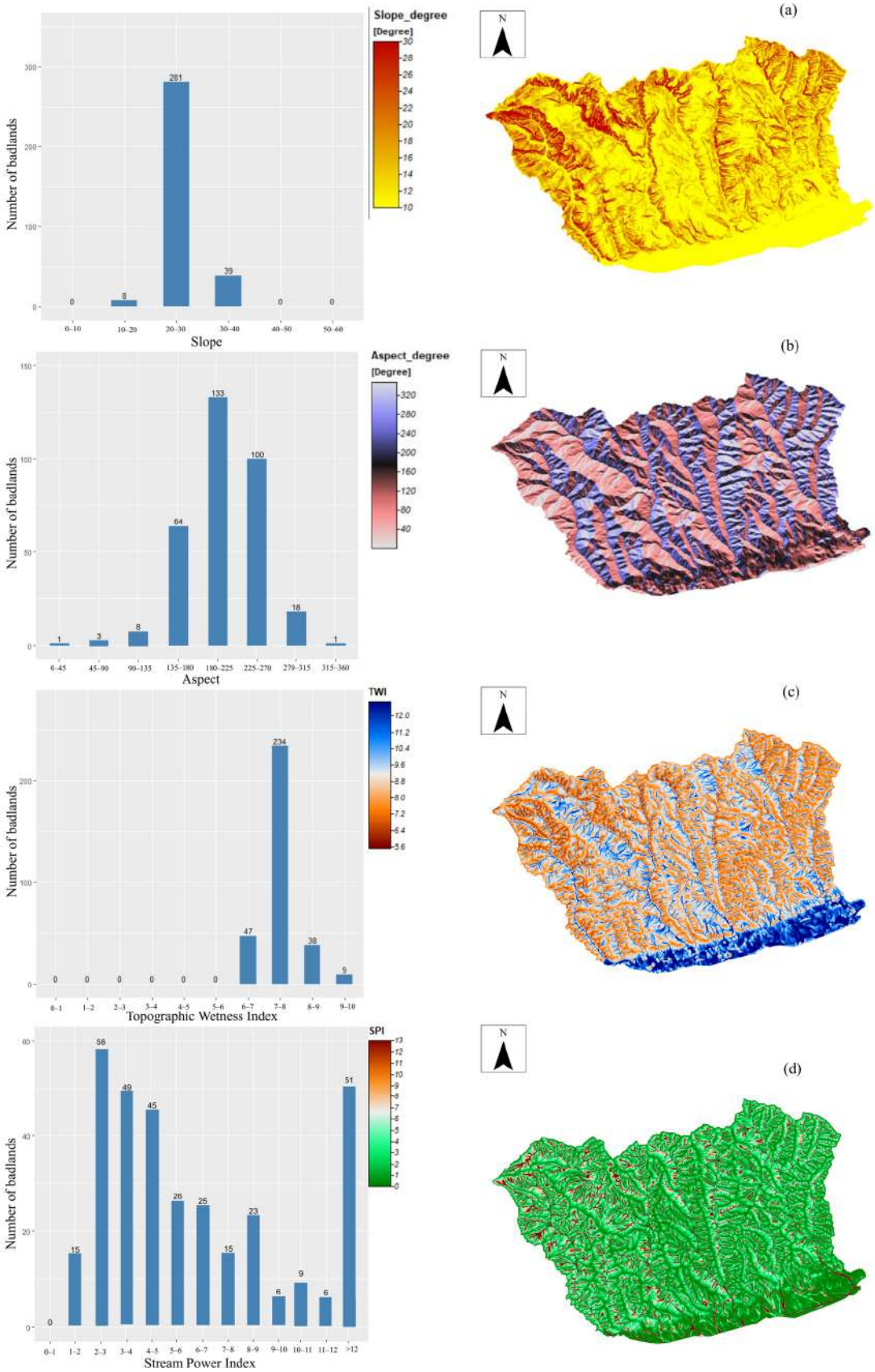

Figure 8. Morphometric parameters calculated from DEM 10 m data; (**a**) slope; (**b**) aspect; (**c**) Topographic Wetness Index; (**d**) Stream Power Index.

According to the classification used by Gallart et al. [28], the investigated area falls within semi-arid and humid conditions, and consequently the amount of vegetation is controlled by the climatic conditions. In this type of climate, the vegetation cover may play an important role in contrasting the erosion rate.

Concerning the badlands area variation trend, a temporal evolution of both the rainfall amount and intensity as well as the land use change was evaluated. Regarding the rainfall amount, a slight decrease in the mean annual precipitation trend can be observed (Figure 9). Conversely, by evaluating the 99th percentile (Figure 10), a precipitation intensity increase can be observed.

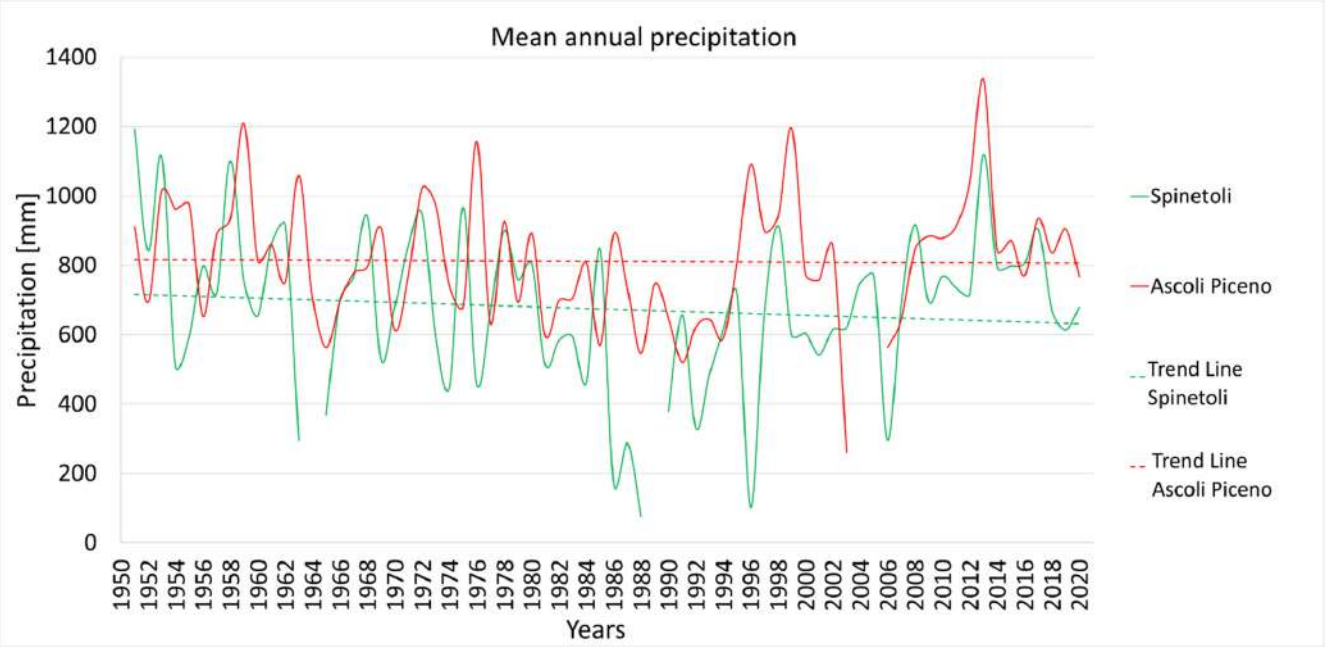

Figure 9. Annual mean precipitation for Spinetoli and Ascoli Piceno stations.

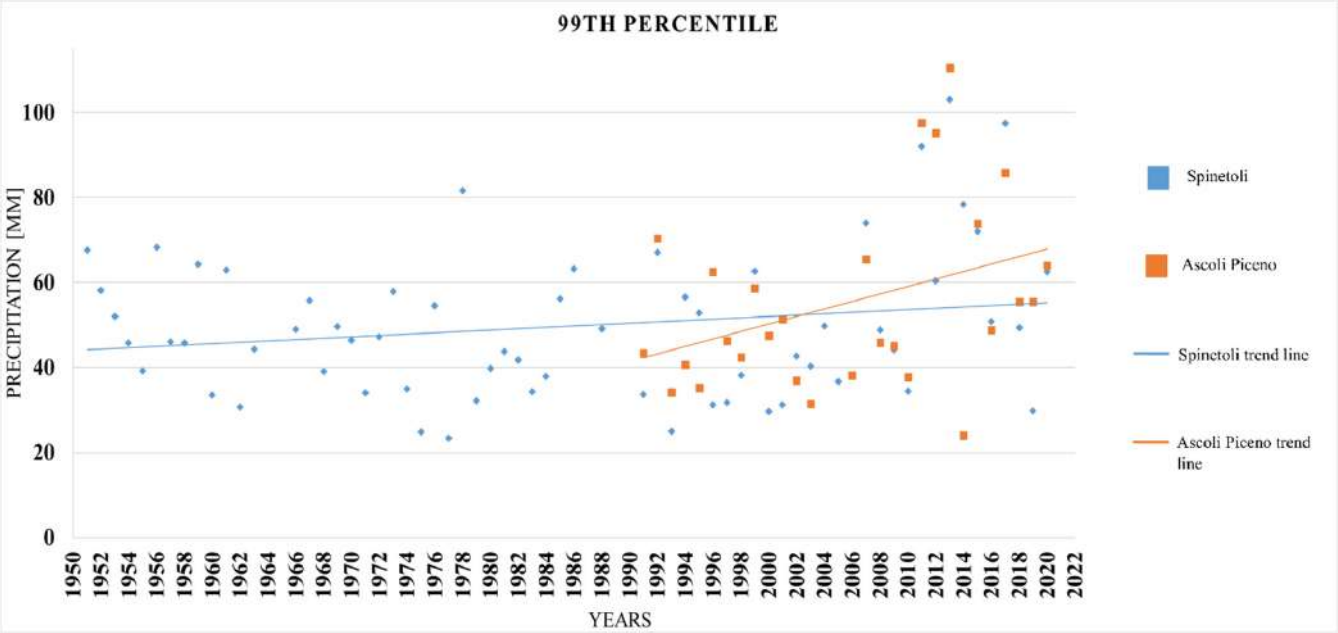

Figure 10. A 99th percentile analysis for Spinetoli and Ascoli Piceno stations.

Regarding the land use changes, the analysis of the data (Table 1) showed that agricultural areas and vineyards increased considerably by 21.77 and 5.51%, respectively. On the contrary, the forests and natural grassland areas significantly decreased by 2.43 and 37.77%, respectively (Table 1).

Table 1. Land use changes over two periods in 1990 and 2016.

CLC CODE	Legend_3Level	AREA 1990	AREA 2018	1990%	2018%	Δ (1990–2018)
111	Continuous urban fabric	0.00	0.62	0.00	0.37	0.37
112	Discontinuous urban fabric	2.04	6.36	1.22	3.80	2.58
121	Industrial or commercial units	1.02	3.02	0.61	1.80	1.20
122	Road and rail networks and associated land	5.86	0.00	3.50	0.00	−3.50
123	Port areas	0.11	0.00	0.07	0.00	−0.07
131	Mineral extraction sites	1.56	0.31	0.93	0.18	−0.75
132	Dump sites	0.01	0.00	0.01	0.00	−0.01
142	Sport and leisure facilities	0.50	0.00	0.30	0.00	−0.30
211	Non-irrigated arable land	8.25	44.71	4.92	26.70	21.77
221	Vineyards	0.00	9.24	0.00	5.51	5.51
231	Pastures	3.07	0.00	1.83	0.00	−1.83
242	Complex cultivation patterns	3.51	65.88	2.10	39.34	37.24
243	Land principally occupied by agriculture, with significant areas of natural vegetation	5.64	9.53	3.37	5.69	2.32
311	Broad-leaved forest	19.67	8.18	11.74	4.89	−6.86
312	Coniferous forest	8.62	0.00	5.15	0.00	−5.15
313	Mixed forest	63.26	0.00	37.77	0.00	−37.77
321	Natural grasslands	4.07	0.00	2.43	0.00	−2.43
324	Transitional woodland-shrub	12.64	13.21	7.55	7.89	0.34
331	Beaches, dunes, sands	5.43	0.00	3.24	0.00	−3.24
332	Bare rocks	0.00	2.74	0.00	1.63	1.63
333	Sparsely vegetated areas	0.00	3.68	0.00	2.20	2.20
411	Inland marshes	4.08	0.00	2.44	0.00	−2.44
511	Water courses	17.90	0.00	10.69	0.00	−10.69
512	Water bodies	0.21	0.00	0.13	0.00	−0.13

The NDVI index, on the other hand, shows a discrete increase in the presence of vegetation from 1988 to 2016 (about 17.8%). The NDVI images were classified into three classes as follows [81–84]: (i) no vegetation for values less than 0.2; (ii) medium vegetation for values between 0.2 and 0.4; (iii) dense vegetation cover for values of more than 0.4. The analysis showed that in general, the spatial extent of green cover in the study area increased from 108 km^2 in 1988 (Figure 11a,b) to 135 km^2 in 2016 (Figure 11c,d). In particular, the dense vegetation cover (class 3) increased in the study area from 31 km^2 (19%) in 1988 to 52 km^2 (32%) in 2016 (Figure 11e). The same figure shows that the class of low vegetation (class 1) areas decreased from 36% of the total investigated area in 1988 to 19% in 2016 (Figure 11e). Moreover, the green vegetation was enhanced within the badlands areas (Figure 12a,b). The area of dense vegetation increased from 1988 to 2016, from 11% to 18% of the total badland areas, while the low-vegetation areas in badlands have decreased from 45% to 29% (Figure 12c).

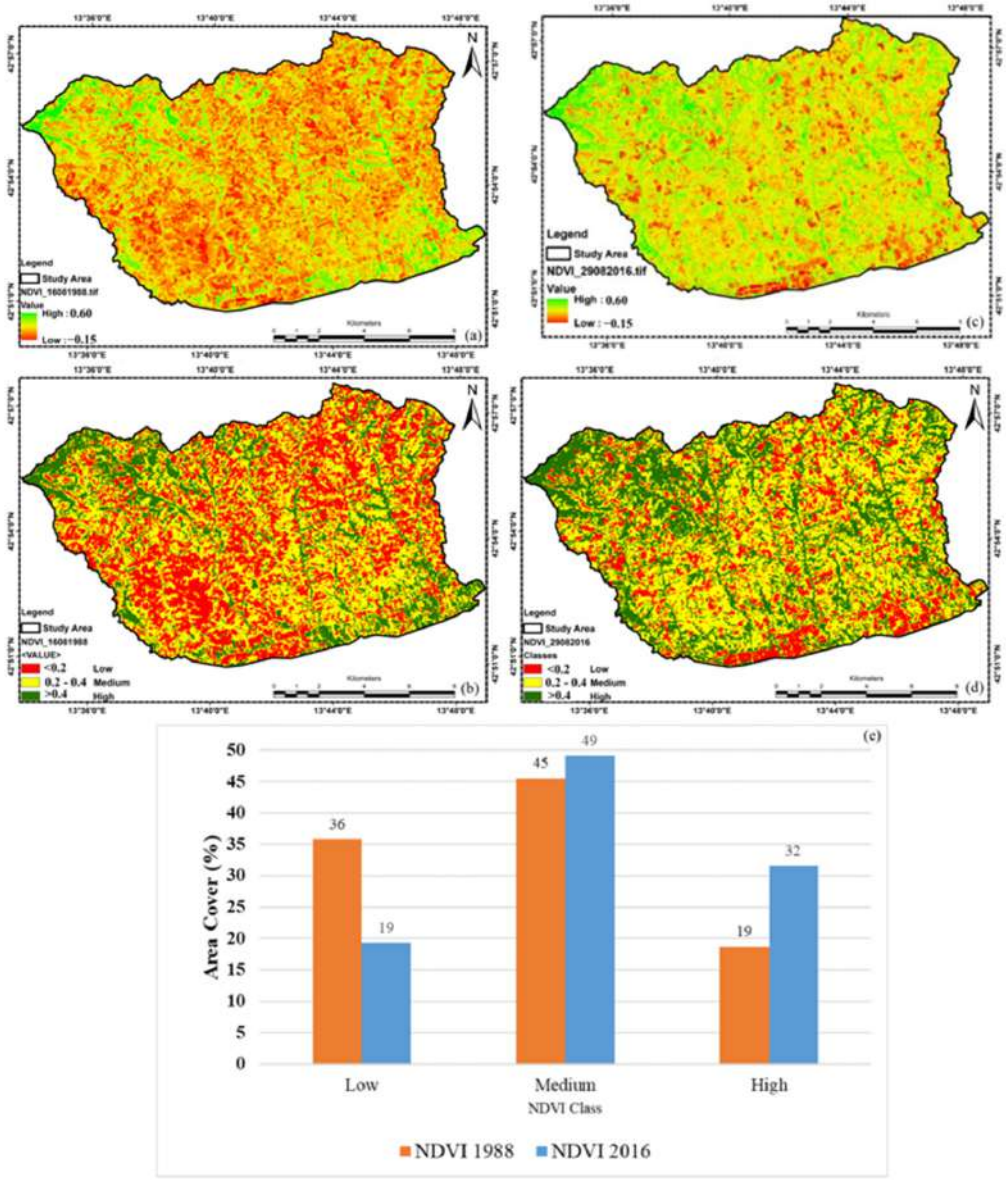

Figure 11. Spatial distribution of NDVI values for the analyzed periods: (**a**,**b**) NDVI values and NDVI classes in 1988 and (**c**,**d**) NDVI values and NDVI classes in 2016. (**e**) Percentage of area in each year.

Even if in the study area a general increase in agricultural fields and vineyards was detected, the NDVI data confirmed that the study area is becoming greener. This trend of vegetation is occurring along with land cover changes (Table 1) that are stabilizing the areas within and around the badlands.

The increase in vegetation cover confirms a tendency towards stabilization of the study area and consequently the presence of less intense erosion processes. This trend is associated with significant changes in land use, which is in contrast with the observations made by Bosino et al. [9]. In fact, in the Oltrepo Pavese area (Northern Apennines), a decrease in the agricultural area and increases in forests and annual green cover were reported, while in the study area proposed here an opposite trend was observed (Table 1). However, the shrinking trend of the badlands areas is due to an increase in dense vegetation, as observed in both study areas. This fact can be explained by the steeper slope characteristics of the badlands, making them unusable for agricultural purposes.

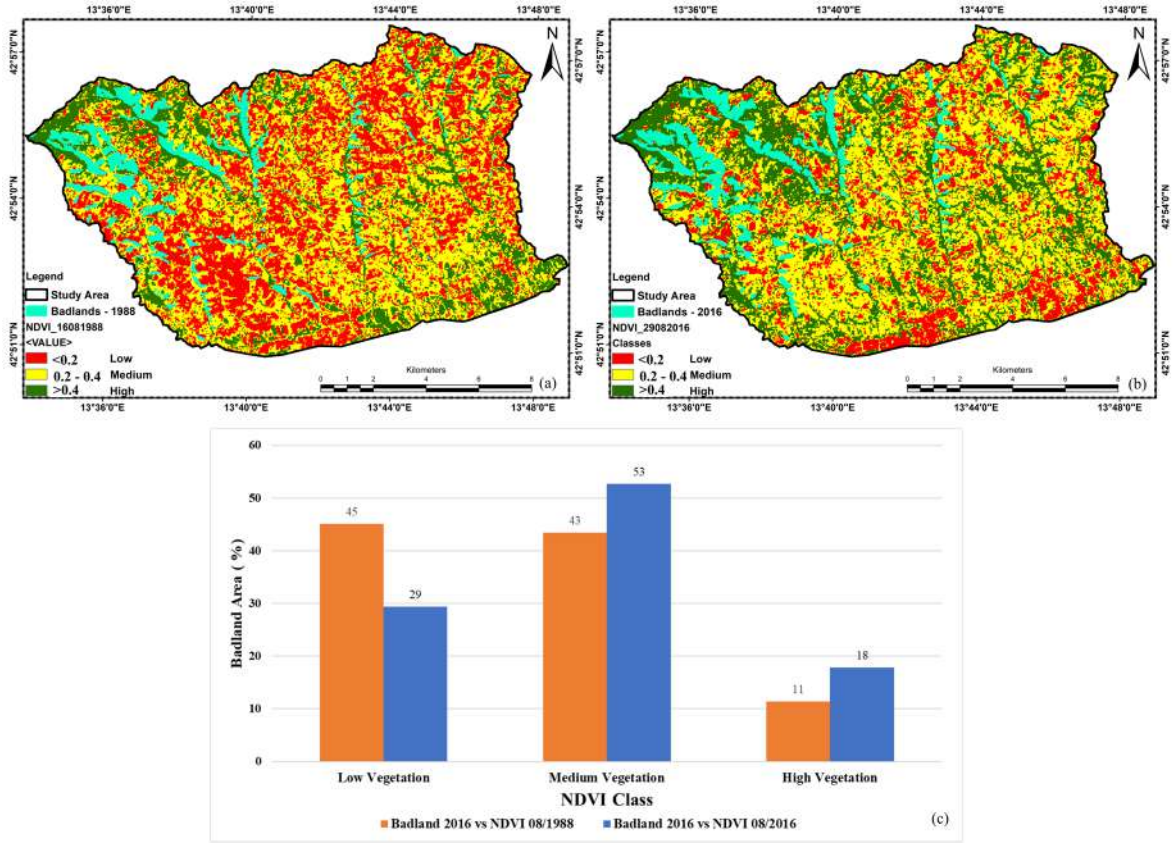

Figure 12. Spatial distribution of NDVI values within badlands areas: (**a**) 1988; (**b**) 2016; (**c**) percentage of area in each year.

In addition, the minimum decrease in precipitation amount also reduces desertification and contrasting soil erosion and promotes the development of vegetation. On the other hand, the precipitation amount is still sufficient to trigger shallow landslides and mud flows. This was also confirmed by the analysis of the precipitation percentiles. In particular, the 99th percentile, which was the one taken as a reference for heavy precipitation (Figure 10), shows that rainfall has evolved as "extreme events", even if it has slightly decreased over time (Figure 9). Therefore, as already mentioned before, this favors the development of mud flows and small shallow landslides, which are accumulating in the badlands' accumulation zones, helping to reduce the slope and the rooting of vegetation (Figure 13).

These observations were also confirmed by the analysis of the NDVI values, which showed an increase in vegetated areas to the detriment of the badlands. The results of this work highlight progressive changes in morphology for the badlands and in the percentages of herbaceous and shrubby vegetation, which characterize these landforms during different evolution phases. Finally, the changes in badlands morphology are mainly associated with land use changes and rainfall erosivity variation that occurred in the last 31 years.

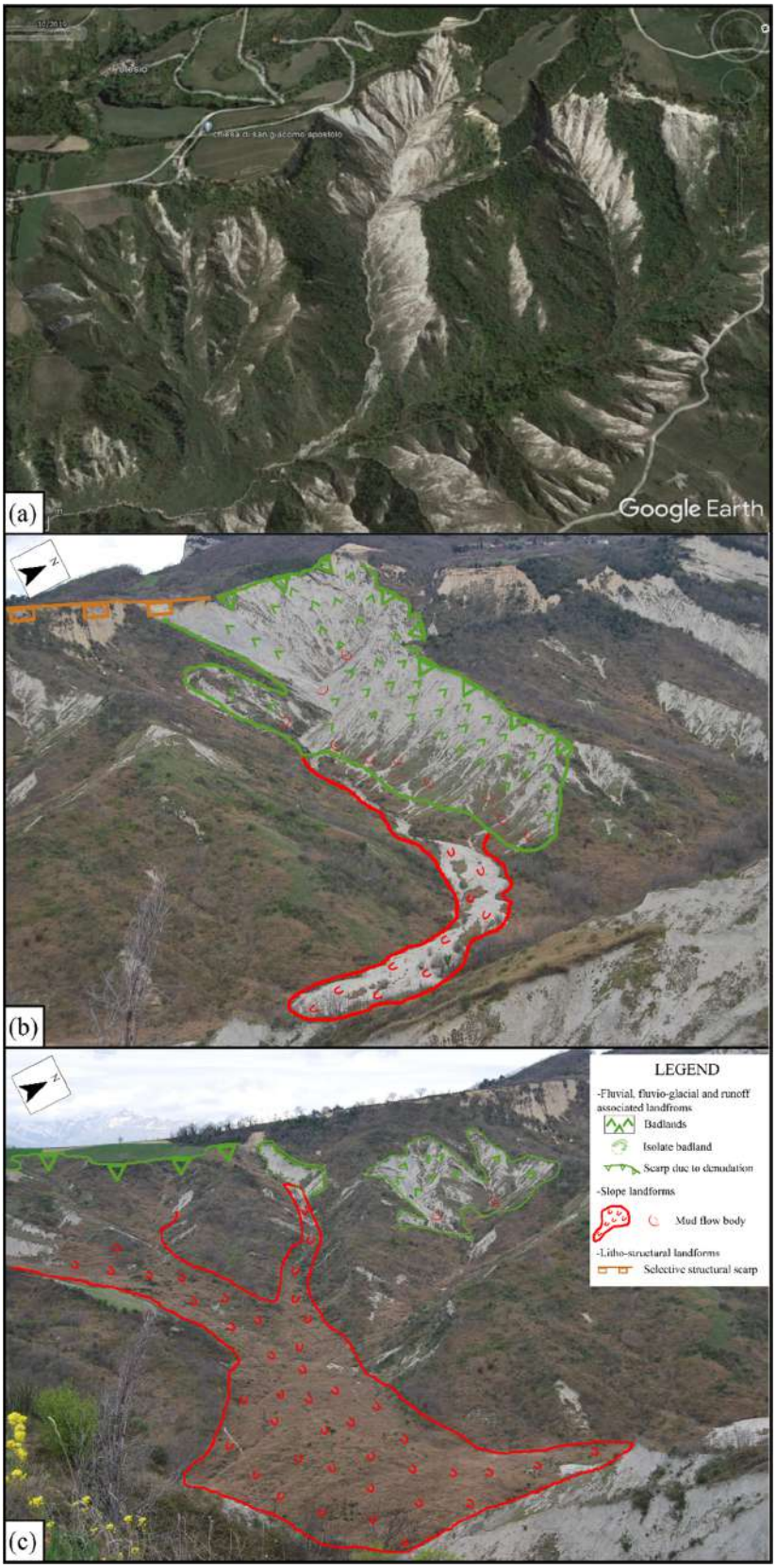

Figure 13. (**a**) Mud flow associated with type A and type B badlands areas. Image from Google Earth, October 2019. (**b**) Recent mud flow body associated with type A badlands, April 2022. (**c**) Vegetated mud flow body and revegetated interfluve slopes on type B badlands, April 2022.

5. Conclusions

In this article, we surveyed and classified the badlands in the area north of the Tronto River Basin. In total, 328 badlands were identified for a total area (in 2016) of 7.04 km^2. Badlands were classified from morphological, morphometrical, and lithological perspectives. From the morphological observations, a predominance of type B badlands was observed in the study area. These badlands represent the natural evolution of type A badlands under actual climatic and land use influences. In addition, from the field observation, it was evident that several type A badlands have undergone a revegetation process. This was also confirmed by the NDVI analysis, which highlighted the stabilization trend. Furthermore, this study shows that the reduction in badlands area was caused primarily by natural processes, and to a lesser extent by anthropogenic processes. A small reduction in average annual precipitation causes a slight decrease in running water processes favoring revegetation. However, as discussed by Nadal-Romero et al. [31], a decrease in annual precipitation, correlated with an increase in its intensity, could produce lower runoff volumes but greater erosion rates. The material eroded during a storm event is accumulated in the foothills and in the badlands' interfluves, reducing the slope and favoring the growth of vegetation in these areas under actual climatic conditions. In addition, active and more or less vegetated mud flow bodies were associated with several badlands landforms, indicating that different processes are still active. However, more detailed studies will have to be performed in the future regarding the physical and chemical properties of the soils of these badlands in order to understand the relations between badlands morphodynamics and mud flow associations. In conclusion, this study confirms that the badlands of the Tronto River Basin are shrinking due to a combination of natural and anthropic actions in the last 31 years, highlighting a general trend observed in other parts of Italy.

Author Contributions: All authors contributed to the study conception and design. Material preparation and data collection and analysis were performed by M.B., A.O., and A.B. The first draft of the manuscript was written by A.B., and all authors commented on previous versions of the manuscript. All authors have read and agreed to the published version of the manuscript.

Funding: The authors declare that no funds, grants, or other support were received during the preparation of this manuscript.

Data Availability Statement: The data provided within the manuscript are available on request from the authors.

Acknowledgments: The authors would like to thank the Consorzio di Bonifica delle Marche for kindly providing the 2016 orthophotos, and to Davide Abu El Khair for the grain size analysis.

Conflicts of Interest: The authors declare no conflict of interest.

References

1. Jie, C.; Chen, J.-Z.; Tan, M.-Z.; Gong, Z.-T. Soil degradation: A global problem endangering sustainable development. *J. Geogr. Sci.* **2002**, *12*, 243–252. [CrossRef]
2. van Leeuwen, C.C.E.; Cammeraat, E.L.H.; de Vente, J.; Boix-Fayos, C. The evolution of soil conservation policies targeting land abandonment and soil erosion in Spain: A review. *Land Use Policy* **2019**, *83*, 174–186. [CrossRef]
3. Harvey, A. Badlands. In *Encyclopedia of Geomorphology*; Goudie, A., Ed.; Psychology Press: London, UK, 2004; pp. 45–47.
4. Caraballo-Arias, N.A.; Ferro, V. Assessing, measuring and modelling erosion in calanchi areas: A review. *J. Agric. Eng.* **2016**, *47*, 181–190. [CrossRef]
5. Azzi, G. I fenomeni della erosione nelle Argille Azzurre del Pliocene nel bacino del Santerno (Romagna). *Boll. Soc. Geogr. Ital.* **1912**, *II*, 111–114.
6. Castiglioni, B. Osservazioni sui calanchi appenninici. *Boll. Soc. Geol. Ital.* **1933**, *LII*, 357–360.
7. Castiglioni, B. Ricerche morfologiche nei terreni pliocenici dell'Italia centrale. *Pubbl. Ist. Geogr. Univ. Rome* **1935**, *Ser. A*, 160.
8. Bianchini, S.; Del Soldato, M.; Solari, L.; Nolesini, T.; Pratesi, F.; Moretti, S. Badland susceptibility assessment in Volterra municipality (Tuscany, Italy) by means of GIS and statistical analysis. *Environ. Earth Sci.* **2016**, *75*, 889. [CrossRef]
9. Bosino, A.; Omran, A.; Maerker, M. Identification, characterisation and analysis of the Oltrepo Pavese calanchi in the Northern Apennines (Italy). *Geomorphology* **2019**, *340*, 53–66. [CrossRef]

10. Ciccacci, S.; Galiano, M.; Roma, M.A.; Salvatore, M.C. Morphological analysis and erosion rate evaluation in badlands of Radicofani area (Southern Tuscany—Italy). *Catena* **2008**, *74*, 87–97. [CrossRef]
11. Coratza, P.; Vandelli, V.; Soldati, M. Environmental rehabilitation linking natural and industrial heritage: A Master Plan for dismissed quarry areas in the Emilia Apennines (Italy). *Environ. Earth Sci.* **2018**, *77*, 455. [CrossRef]
12. Coratza, P.; Parenti, C. Controlling Factors of badland morphological changes in the Emilia Apennines (Northern Italy). *Water* **2021**, *13*, 539. [CrossRef]
13. Demangeot, J. Géomorphologie des Abruzzes adriatiques. In *Éditions du Centre National de la Recherche Scientifique*; Centre National de la Recherche Scientifique: Paris, France, 1965; pp. 188–189.
14. Dramis, F.; Gentili, B.; Coltorti, M.; Cherubini, C. Osservazioni geomorfologiche sui calanchi marchigiani. *Geogr. Fis. Din. Quat.* **1982**, *5*, 38–45.
15. Dramis, F.; Gentili, B.; Pieruccini, U. La degradazione dei versanti nel bacino del Sentino (Appennino Umbro-Marchigiano). *Stud. Geol. Camerti* **1976**, *2*, 45–72.
16. Karmeshu, N. Trend Detection in Annual Temperature & Precipitation Using the Mann Kendall Test—A Case Study to Assess Climate Change on Select States in the Northeastern United States. Ph.D. Thesis, University of Pennsylvania, Philadelphia, PA, USA, August 2012; pp. 1–33.
17. Maerker, M.; Bosino, A.; Scopesi, C.; Giordani, P.; Firpo, M.; Rellini, I. Assessment of calanchi and rill-interrill erosion susceptibility in northern Liguria, Italy: A case study using a probabilistic modelling framework. *Geoderma* **2020**, *371*, 114367. [CrossRef]
18. Rodolfi, G.; Frascati, F. Cartografia di base per la programmozione degli interventi in aree marginali (Area rappresentativa Alta val D'era). *Ann. Dell'istituto Sper. Per Studio Dif. Suolo Firenze* **1979**, *10*.
19. Bosino, A.; Giordani, P.; Quénéhervé, G.; Maerker, M. Assessment of calanchi and rill–interrill erosion susceptibilities using terrain analysis and geostochastics: A case study in the Oltrepo Pavese, Northern Apennines, Italy. *Earth Surf. Process. Landf.* **2020**, *45*, 3025–3041. [CrossRef]
20. Bouma, N.A.; Imeson, A.C. Investigation of relationships between measured field indicators and erosion processes on badland surfaces at Petrer, Spain. *Catena* **2000**, *40*, 147–171. [CrossRef]
21. Brandolini, P.; Pepe, G.; Capolongo, D.; Cappadonia, C.; Cevasco, A.; Conoscenti, C.; Marsico, A.; Vergari, F.; Del Monte, M. Hillslope degradation in representative Italian areas: Just soil erosion risk or opportunity for development? *Land Degrad. Dev.* **2018**, *29*, 3050–3068. [CrossRef]
22. Bucciante, M. Sulla distribuzione geografica dei calanchi in Italia. *L'Universo* **1922**, *3*, 585–605.
23. Buccolini, M.; Coco, L.; Cappadonia, C.; Rotigliano, E. Relationships between a new slope morphometric index and calanchi erosion in northern Sicily, Italy. *Geomorphology* **2012**, *149–150*, 41–48. [CrossRef]
24. Buccolini, M.; Coco, L. The role of the hillside in determining the morphometric characteristics of "calanchi": The example of Adriatic central Italy. *Geomorphology* **2010**, *123*, 200–210. [CrossRef]
25. Cappadonia, C.; Coco, L.; Buccolini, M.; Rotigliano, E. From slope morphometry to morphogenetic processes: An integrated approach of field survey, geographic information system morphometric analysis and statistics in Italian Badlands. *Land Degrad. Dev.* **2016**, *27*, 851–862. [CrossRef]
26. Caraballo-Arias, N.A.; Conoscenti, C.; Di Stefano, C.; Ferro, V. Testing GIS-morphometric analysis of some Sicilian badlands. *Catena* **2014**, *113*, 370–376. [CrossRef]
27. Del Monte, M. The typical badlands landscapes between the tyrrhenian sea and the tiber river. In *Landscapes and Landforms of Italy*; Springer: Berlin/Heidelberg, Germany, 2017; pp. 281–291. [CrossRef]
28. Gallart, F.; Solé-Benet, A.; Puigdefábregas, J.; Lázaro, R. Badland systems in the Mediterranean. In *Dryland Rivers: Hydrology and Geomorphology of Semi-Arid Channels*; Wiley: New York, NY, USA, 2002; pp. 299–326.
29. Stark, M.; Neugirg, F.; Kaiser, A.; Della Seta, M.; Schmidt, J.; Becht, M.; Haas, F. Calanchi badlands reconstructions and long-term change detection analysis from historical aerial and UAS image processing. *J. Geomorphol.* **2020**, 1–24. [CrossRef]
30. Alexander, D. Difference between' calanchi' and ' biancane' badlands in Italy. In *Badland Geomorphology and Piping*; 1982; pp. 71–87.
31. Nadal-Romero, E.; Rodríguez-Caballero, E.; Chamizo, S.; Juez, C.; Cantón, Y.; García-Ruiz, J.M. Mediterranean badlands: Their driving processes and climate change futures. *Earth Surf. Process. Landf.* **2021**, *47*, 17–31. [CrossRef]
32. Alexander, R.W.; Calvo, A. The influence of lichens on slope processes in some Spanish Badlands. *Veg. Eros.* **1990**, 385–398.
33. Bosino, A.; Szatten, D.A.; Omran, A.; Crema, S.; Crozi, M.; Becker, R.; Bettoni, M.; Schillaci, C.; Maerker, M. Assessment of suspended sediment dynamics in a small ungauged badland catchment in the Northern Apennines (Italy) using an in-situ laser diffraction method. *Catena* **2022**, *209*, 105796. [CrossRef]
34. Clarke, M.L.; Rendell, H.M. Climate-driven decrease in erosion in extant Mediterranean badlands. *Earth Surf. Process. Landf.* **2010**, *35*, 1281–1288. [CrossRef]
35. Nadal-Romero, E.; Martínez-Murillo, J.F.; Vanmaercke, M.; Poesen, J. Scale-dependency of sediment yield from badland areas in Mediterranean environments. *Prog. Phys. Geogr.* **2011**, *35*, 297–332. [CrossRef]
36. Gallart, F.; Pérez-Gallego, N.; Latron, J.; Catari, G.; Martínez-Carreras, N.; Nord, G. Short- and long-term studies of sediment dynamics in a small humid mountain Mediterranean basin with badlands. *Geomorphology* **2013**, *196*, 242–251. [CrossRef]
37. Moreno-de Las Heras, M.; Gallart, F. *The Origin of Badlands*; Elsevier Inc.: Amsterdam, The Netherlands, 2018; ISBN 9780128130544.

38. García-Ruiz, J.M.; Nadal-Romero, E.; Lana-Renault, N.; Beguería, S. Erosion in Mediterranean landscapes: Changes and future challenges. *Geomorphology* **2013**, *198*, 20–36. [CrossRef]
39. Díaz, V.; Mongil, J.; Navarro, J. Topographical surveying for improved assessment of sediment retention in check dams applied to a Mediterranean badlands restoration site (Central Spain). *J. Soils Sediments* **2014**, *14*, 2045–2056. [CrossRef]
40. Ambrosetti, P.; Carraro, F.; Deiana, G.; Dramis, F. Il sollevamento dell'Italia centrale tra il Pleistocene inferiore e il Pleistocene medio. *PF Geodin.-CNR* **1982**, *513*, 219–223.
41. Bisci, C.; Dramis, F.; Gentili, B. Badlands on the adriatic side of central Italy. *Geookoplus* **1992**, *3*, 55–58.
42. Phillips, C.P. The badlands of Italy: A vanishing landscape? *Appl. Geogr.* **1998**, *18*, 243–257. [CrossRef]
43. Buccolini, M.; Gentili, B.; Materazzi, M.; Aringoli, D.; Pambianchi, G.; Piacentini, T. Human impact and slope dynamics evolutionary trends in the monoclinal relief of Adriatic area of central Italy. *Catena* **2007**, *71*, 96–109. [CrossRef]
44. Buccolini, M.; D'Alessandro, L.; Fazzini, M.; Gentili, B.; Materazzi, M.; Piacentini, T.; Aringoli, D. Aspetti morfoevolutivi del settore periadriatico marchigiano-abruzzese (Italia centrale). In *Erosione Idrica in Ambiente Mediterraneo: Valutazione Diretta e Indiretta in Aree Sperimentali e Bacini Idrografici*; Brigat, G., Ed.; Brigati: Camerino, Italy, 2006; pp. 159–175.
45. Buccolini, M.; Coco, L. MSI (morphometric slope index) for analyzing activation and evolution of calanchi in Italy. *Geomorphology* **2013**, *191*, 142–149. [CrossRef]
46. Ciccacci, S.; Fredi, P.; Lupia Palmieri, E.; Pugliese, F. Contributo dell'analisi geomorfica quantitativa alla valutazione dell'entità dell'erosione nei bacini fluviali. *Boll. Soc. Geol. Ital.* **1980**, *99*, 455–516. [CrossRef]
47. Cocco, S.; Brecciaroli, G.; Agnelli, A.; Weindorf, D.; Corti, G. Soil genesis and evolution on calanchi (badland-like landform) of central Italy. *Geomorphology* **2015**, *248*, 33–46. [CrossRef]
48. Farabollini, P.; Scalella, G. Itinerari geoturistici nel comprensorio del Monte dell' Ascensione e dei calanchi Geotouristic routes in Monte Ascensione and badlands district. *Mem. Descr. Cart. Geol. d'Ital.* **2014**, *102*, 57–71.
49. Farabollini, P.; Gentili, B.; Pambianchi, G. Contributo allo studio dei calanchi: Due aree campione nelle Marche. *Stud. Geol. Camerti* **1992**, *12*, 105–115.
50. Moretti, S.; Rodolfi, G. A typical "calanchi" landscape on the Eastern Apennine margin (Atri, Central Italy): Geomorphological features and evolution. *Catena* **2000**, *40*, 217–228. [CrossRef]
51. Castaldi, F.; Chiocchini, U. Effects of land use changes on badland erosion in clayey drainage basins, Radicofani, Central Italy. *Geomorphology* **2012**, *169–170*, 98–108. [CrossRef]
52. Soldati, M.; Parenti, C.; Coratza, P. Geodiversity through time: Changing badland landscapes due to anthropogenic and climatic forcing in the Northern Apennines (Italy). In Proceedings of the 22nd EGU General Assembly, Online Event. 4–8 May 2020; p. 19319.
53. Salvini, R. Analisi morfometriche delle Crete Senesi mediante remote sensing e GIS. Morphometric analysis of Crete Senesi by means of remote sensing and GIS. *Mem. Descr. Della Carta Geol. D'Ital.* **2008**, *78*, 245–252.
54. D'Intino, J.; Buccolini, M.; Di Nardo, E.; Esposito, G.; Miccadei, E. Geomorphology of the Anversa degli Abruzzi badlands area (Central Apennines, Italy). *J. Maps* **2020**, *16*, 488–499. [CrossRef]
55. Ciccacci, S.; Galiano, M.; Roma, M.A.; Salvatore, M.C. Morphodynamics and morphological changes of the last 50 years in a badland sample area of Southern Tuscany (Italy). *Z. Geomorphol.* **2009**, *53*, 273. [CrossRef]
56. Della Seta, M.; Del Monte, M.; Fredi, P.; Lupia Palmieri, E. Space–time variability of denudation rates at the catchment and hillslope scales on the Tyrrhenian side of Central Italy. *Geomorphology* **2009**, *107*, 161–177. [CrossRef]
57. Lugeri, F.R.; Farabollini, P.; De Pascale, F.; Lugeri, N.; Lugeri, F.R.; Farabollini, P.; De Pascale, F.; Lugeri, N. PPGIS applied to environmental communication and hazards for a community-based approach: A dualism in the Southern Italy "calanchi" landscape. *AIMS Geosci.* **2021**, *7*, 490–506. [CrossRef]
58. Maccherini, S.; Marignani, M.; Gioria, M.; Renzi, M.; Rocchini, D.; Santi, E.; Torri, D.; Tundo, J.; Honnay, O. Determinants of plant community composition of remnant biancane badlands: A hierarchical approach to quantify species-environment relationships. *Appl. Veg. Sci.* **2011**, *14*, 378–387. [CrossRef]
59. Kottek, M.; Grieser, J.; Beck, C.; Rudolf, B.; Rubel, F. World map of the Köppen-Geiger climate classification updated. *Meteorol. Z.* **2006**, *15*, 259–263. [CrossRef]
60. Peel, M.C.; Finlayson, B.L.; McMahon, T.A. Updated world map of the Köppen-Geiger climate classification. *Hydrol. Earth Syst. Sci.* **2007**, *11*, 1633–1644. [CrossRef]
61. Gentilucci, M.; Materazzi, M.; Pambianchi, G.; Burt, P.; Guerriero, G. Temperature variations in Central Italy (Marche region) and effects on wine grape production. *Theor. Appl. Climatol.* **2020**, *140*, 303–312. [CrossRef]
62. Centamore, E.; Deiana, G.; Micarelli, A.; Potetti, M. Il Trias-Paleogene delle Marche. In *Studi Geologici Camerti, Volume Speciale "La Geologia delle Marche"*; Università di Camerino: Camerino, Italy, 1986; pp. 9–27.
63. Cantalamessa, G.; Centamore, E.; Didaskalou, P.; Micarelli, A.; Napoleone, G.; Potetti, M. Elementi di correlazione nella successione marina plio-pleistocenica del bacino periadriatico marchigiano. *Studi Geol. Camerti Nuova Ser.* **2002**, *1*, 33–49.
64. Centamore, E.; Deiana, G. *La Geologia Delle Marche*; Univerisità di Camerino, Ed.; Università di Camerino: Camerino, Italy, 1986.
65. Cantalamessa, G.; Centamore, E.; Chiocchini, U.; Colalongo, M.L.; Micarelli, A.; Nanni, T.; Pasini, G.; Potetti, M.; Ricci Lucchi, F.; Cristallini, C.; et al. Il Plio-Pleistocene delle Marche. In *Studi Geologici Camerti, Colume Spec. "La Geol. delle Marche"*; Università di Camerino: Camerino, Italy, 1986; pp. 61–81.

66. Gentili, B.; Pambianchi, G.; Aringoli, D.; Cilla, G.; Farabollini, P.; Materazzi, M. Rapporti tra deformazioni fragili plio-quaternarie e morfogenesi gravitativa nella fascia alto-collinare delle marche centro-meridionali. *Stud. Geol. Camerti* **1995**, *1*, 421–435.
67. Invernizzi, C.; Cacciamani, A.; Dignani, A. Jointing nell'area marchigiana esterna: Caratteristiche geometriche e significato strutturale. *Studi Geol. Camerti* **1992**, 137–144.
68. Paliaga, G. Erosion Triangular facets as markers of order in an open dissipative system. *Pure Appl. Geophys.* **2015**, *172*, 1985–1997. [CrossRef]
69. Pierantoni, P.; Deiana, G.; Galdenzi, S. Stratigraphic and structural features of the sibillini mountains (Umbria-Marche Apennines, Italy). *Ital. J. Geosci.* **2013**, *132*, 497–520. [CrossRef]
70. Vergari, F. Assessing soil erosion hazard in a key badland area of Central Italy. *Nat. Hazards* **2015**, *79*, 71–95. [CrossRef]
71. Moore, I.D.; Grayson, R.B.; Ladson, A.R. Digital terrain modelling: A review of hydrological, geomorphological, and biological applications. *Hydrol. Process.* **1991**, *5*, 3–30. [CrossRef]
72. Conrad, O.; Bechtel, B.; Bock, M.; Dietrich, H. System for automated geoscientific analyses (SAGA) v. 2.1. 4. *Geosci. Model Dev.* **2015**, *8*, 1991–2007. [CrossRef]
73. Wang, L.; Liu, H. An efficient method for identifying and filling surface depressions in digital elevation models for hydrologic analysis and modelling. *Int. J. Geogr. Inf. Sci.* **2006**, *20*, 193–213. [CrossRef]
74. Emori, S.; Brown, S.J. Dynamic and thermodynamic changes in mean and extreme precipitation under changed climate. *Geophys. Res. Lett.* **2005**, *32*, 1–5. [CrossRef]
75. Anagnostopoulou, C.; Tolika, K. Extreme precipitation in Europe: Statistical threshold selection based on climatological criteria. *Theor. Appl. Climatol.* **2012**, *107*, 479–489. [CrossRef]
76. Wasko, C.; Sharma, A. Quantile regression for investigating scaling of extreme precipitation with temperature. *Water Resour. Res.* **2014**, *50*, 3608–3614. [CrossRef]
77. Pińskwar, I. Complex changes of extreme precipitation in the warming climate of Poland. *Int. J. Climatol.* **2021**, *42*, 817–833. [CrossRef]
78. Najafi, M.R.; Moazami, S. Trends in total precipitation and magnitude–frequency of extreme precipitation in Iran, 1969–2009. *Int. J. Climatol.* **2016**, *36*, 1863–1872. [CrossRef]
79. Buccolini, M.; Bufalini, M.; Coco, L.; Materazzi, M.; Piacentini, T. Small catchments evolution on clayey hilly landscapes in Central Apennines and northern Sicily (Italy) since the Late Pleistocene. *Geomorphology* **2020**, *363*, 107206. [CrossRef]
80. Capolongo, D.; Diodato, N.; Mannaerts, C.M.; Piccarreta, M.; Strobl, R.O. Analyzing temporal changes in climate erosivity using a simplified rainfall erosivity model in Basilicata (Southern Italy). *J. Hydrol.* **2008**, *356*, 119–130. [CrossRef]
81. Weier, J.; Herring, D. Measuring Vegetation (NDVI & EVI). 2000. Available online: https://earthobservatory.nasa.gov/Features/MeasuringVegetation/measuring_vegetation_1.php (accessed on 19 November 2021).
82. Mohajane, M.; Essahlaoui, A.; Oudija, F.; El Hafyani, M.; El Hmaidi, A.; El Ouali, A.; Randazzo, G.; Teodoro, A. Land use/land cover (LULC) using landsat data series (MSS, TM, ETM^{+} and OLI) in Azrou Forest, in the Central Middle Atlas of Morocco. *Environments* **2018**, *5*, 131. [CrossRef]
83. Hashim, H.; Abd Latif, Z.; Adnan, N. Urban Vegetation Classification with Ndvi Threshold Value Method with very High Resolution (vhr) Pleiades imagery. *Int. Arch. Photogramm. Remote Sens. Spat. Inf. Sci.* **2019**, *42*, 237–240. [CrossRef]
84. Sahebjalal, E.; Dashtekian, K. Analysis of land use-land covers changes using normalized difference vegetation index (NDVI) differencing and classification methods. *Afr. J. Agric. Res.* **2013**, *8*, 4614–4622. [CrossRef]